Controlling multiple filaments by relativistic optical vortex beams in plasmas

L. B. Ju,[1,2] T. W. Huang,[3] K. D. Xiao,[3] G. Z. Wu,[1] S. L. Yang,[3] R. Li,[3] Y. C. Yang,[3] T. Y. Long,[3] H. Zhang,[2] S. Z. Wu,[2] B. Qiao,[3] S. C. Ruan,[4] and C. T. Zhou[2,3,4,*]

[1]*Graduate School, China Academy of Engineering Physics, Beijing 100088, People's Republic of China*

[2]*Institute of Applied Physics and Computational Mathematics, Beijing 100094, People's Republic of China*

[3]*HEDPS, Center for Applied Physics and Technology and School of Physics, Peking University, Beijing 100871, People's Republic of China*

[4]*College of Electronic Science and Technology, Shenzhen University, Shenzhen 518060, People's Republic of China*

(Received 27 January 2016; revised manuscript received 15 July 2016; published 2 September 2016)

Filamentation dynamics of relativistic optical vortex beams (OVBs) propagating in underdense plasma is investigated. It is shown that OVBs with finite orbital angular momentum (OAM) exhibit much more robust propagation behavior than the standard Gaussian beam. In fact, the growth rate of the azimuthal modulational instability decreases rapidly with increase of the OVB topological charge. Thus, relativistic OVBs can maintain their profiles for significantly longer distances in an underdense plasma before filamentation occurs. It is also found that an OVB would then break up into regular filament patterns due to conservation of the OAM, in contrast to a Gaussian laser beam, which in general experiences random filamentation.

DOI: 10.1103/PhysRevE.94.033202

I. INTRODUCTION

Long-range propagation of intense short laser pulses in plasma has recently attracted much attention because of its many applications, such as fast ignition (FI) in inertial confinement fusion, laser driven particle accelerators, laser-based radiation sources, etc. [1–7]. In the FI scheme, the ignition laser has to propagate through an underdense plasma before it reaches the critical density. It is therefore desirable for the laser to propagate as large a distance as possible. However, typical lasers tend to suffer from filamentation, hosing, scattering instabilities, etc. [8–20]. The filamentation process is essentially the nonlinear development of modulational instability, which is induced by the beam noise and the nonuniformity of the plasma density. A Gaussian laser beam first experiences the self-focusing stage, then the diffraction process dominates and unstable rings are generated. The ring beams are unstable to the transverse perturbations and would break up randomly. To suppress and control filamentation, one strategy is to introduce anisotropy in the initial laser beam. In an earlier work [12], we proposed a simple and efficient way to mitigate laser filamentation by using an elliptic Gaussian beam. It was found that such a beam breaks up into a regular filament pattern with most of its energy in a central filament.

Another strategy is to use a ring-structured, or Laguerre-Gaussian (LG), optical vortex beam possessing orbital angular momentum (OAM). The azimuthal modulation of the ring structure is nondiffractive and controllable. Moreover, due to OAM conservation, the resulting filamentation instability breaks the ring up in a regular and predictable manner. Light beams with finite OAM were first investigated by Allen *et al.* [21]. They are characterized by having a spiral phase front with OAM in the laser propagation direction. Such beams have been considered in optics, acoustics, electron bunches, etc. [22–24]. In particular, the optical vortex beam has extensive applications in optical microscopy, micromanipulation, quantum information, and astronomy [25–28]. For example, the necklace-ring beam, which is a coherent superposition of two vortex beams, can propagate for a long distance in Kerr media [29], and high-power lasers with finite OAM can propagate in the atmosphere for over hundreds of meters [30–37]. Laser pulses with finite OAM can be implemented by techniques such as mode conversion from Hermite-Gaussian (HG) to LG using spiral phase plates, computer holograms, etc. [38–41]. Recently, the generation of relativistic optical vortex beams using stimulated Raman amplification and a light fan was proposed and investigated [42,43], and the resulting relativistic LG laser beam has stimulated much interest in laser plasma physics [44–46].

Nonlinear propagation of LG laser pulses is important in many areas [22–35,35–37], especially in laser-based applications such as FI [1–7]. In this paper, the filamentation of an intense optical vortex beam with finite OAM in underdense plasma is investigated using a model equation for the relativistic laser propagation. It is shown that the filamentation of an optical vortex beam can be controlled and the number of filaments can be predicted. The growth rate of the azimuthal modulational instability is much decreased with increase of its topological charge. The laser beam can maintain its profile for a long distance in the underdense plasmas before it breaks up into several filaments. In contrast to the random filaments of Gaussian laser beams, the relativistic optical vortex beam breaks up into filaments that are rather robustly distributed with a ring structure that is insensitive to perturbations on the initial beam profile. The paper is organized as follows. In Sec. II, the physical model and the corresponding theoretical analyses are discussed. In Sec. III, multiple filaments of the relativistic optical vortex beam are numerically simulated. The conclusion is given in the final section.

II. PHYSICAL MODEL AND THEORETICAL ANALYSES

To demonstrate the filamentation process of relativistic optical vortex beams in underdense plasmas, a generic relativistic nonlinear Schrödinger equation (RNSE) is performed by considering the relativistic effect and the ponderomotive force. In the slowly varying envelope approximation, the

*zcangtao@iapcm.ac.cn

amplitude of a circularly polarized laser propagation through an underdense plasma can be written as [8–13]

$$2ik_L\frac{\partial}{\partial z}a+\nabla_\perp^2 a+k_p^2\left(1-\frac{n}{\gamma}\right)a=0 \tag{1}$$

in the moving frame of the laser group velocity($\tau=t-z/v_g$). Here a is the slowly varying amplitude vector of a circularly polarized laser beam, ω_L and k_L are, respectively, the mean frequency and wave number of the laser beam, z is the laser propagation direction, m_e is the rest electron mass, and c is the vacuum speed of light. The operator $\nabla_\perp^2=\frac{\partial^2}{\partial x^2}+\frac{\partial^2}{\partial y^2}$ is the Laplace operator in the (x,y) plane, the electron density n is normalized by the equilibrium electron density n_0, and $\gamma=\sqrt{1+|a|^2}$ is the Lorentz factor. The electron density is given as $n=1+k_p^{-2}\nabla_\perp^2(\gamma+\alpha\log_e n)$ to keep the conservation of the charge in plasmas, where $\alpha=T_e/m_ec^2$ is the normalized electron temperature. The above equation is valid for $\alpha\ll 1$ when the thermal motion of electrons is nonrelativistic.

For Eq. (1), there are an infinite number of conserved quantities. The first invariant is the normalized laser power

$$P=\int|a|^2d\vec{r}, \tag{2}$$

where $r=\sqrt{x^2+y^2}$. For the optical vortex beams, the total angular momentum is also conserved, which can be written as

$$L=\frac{i}{2}\int d\vec{r}\left[x\left(a^*\frac{\partial a}{\partial y}-\text{c.c.}\right)-y\left(a^*\frac{\partial a}{\partial x}-\text{c.c.}\right)\right]. \tag{3}$$

One can employ the Laguerre-Gaussian $\text{TEM}_{p,l}$ modes with the radial mode index $p=0$ and the topological charge $l=m$ to describe the optical vortex beam. Its initial profile can be expressed as

$$a(r,\theta,0)=a_0\frac{1}{\sqrt{m!}}\left(\frac{\sqrt{2}r}{r_0}\right)^m\exp\left(-\frac{r^2}{r_0^2}\right)\exp(im\theta), \tag{4}$$

where a_0 and r_0 refer to the amplitude of normalized electric field and beam waist, respectively; m is the topological charge of the optical vortex beam; and θ is the phase angle ranging from 0 to 2π. When m becomes zero, Eq. (4) degenerates to the Gaussian profile. While $m\neq 0$, it represents the ring profile of the optical vortex beam. To get the threshold power for self-focusing, one can use the approximation $a(r)=\sqrt{3}\,\text{sech}(\frac{r-\sqrt{2m}}{\sqrt{2/3}})$ for the stationary solution of Eq. (1) [47,48]. By substituting this solution into Eq. (2), one can get the critical power of self-focusing for relativistic optical vortex beams as $P_{\text{cr}}(m)\approx\frac{8\sqrt{3}m}{3.72}P_{\text{cr}}$, where $P_{\text{cr}}\approx 17(\omega_L/\omega_p)^2$ GW. It is noted that the critical power for self-focusing would increase with the topological charge of the optical vortex beam. The self-focusing distance can be estimated as $z_f=z_R/\sqrt{(\frac{P}{P_{\text{cr}}(m)}-1)}$ [12], which is also increased as m grows. Here $z_R=\pi r_0^2/\lambda$ is the Rayleigh length. In addition, for the laser field that carries a nonzero topological charge, the system of Eq. (1) admits one more important integral of motion, i.e., the angular momentum along the propagation direction $L=\vec{r}\times(\vec{E}\times\vec{B})|_z$. Under the paraxial approximation, one can obtain the total angular momentum of the laser field as $L=mP$, which implies that, once the input power and the topological charge of the beam are determined, the angular momentum of the system is also determined. When an optical vortex beam propagates into the underdense plasmas, this physical quantity would be conserved.

Based on Eq. (1), one can get some important characteristics of the filamentation process of relativistic optical vortex beams in underdense plasmas. The filamentation originates from the nonlinear response of the refractive index. As the initial beam noise develops, it can break up a homogeneous laser beam into small-scale filaments. Particularly for optical vortex beam, its filamentation pattern is a result of the azimuthal modulational instability (AMI) on the rings. The perturbation analysis is carried out on a ring-shaped beam, as given by Eq. (4). The amplitude and radius of the ring beam can be expressed as $a_m=a_0\sqrt{\frac{1}{m!}}m^m\exp(-\frac{m}{2})$ and $r_m=\sqrt{m/2}r_0$, where the laser intensity reaches its maximum. For technical convenience, one can consider the ring beam $a_s(r,\theta,z)$ where its amplitude is zero everywhere along the radial axis, except at $r=r_m$. Here, $a_s(r,\theta,z)$ is defined as the stationary solution of Eq. (1). In this case, the Laplace term is reduced as $\nabla_\perp^2=\frac{1}{r_m^2}\frac{\partial^2}{\partial\theta^2}$. Considering a small azimuthal perturbation on the ring as $\delta a(r,\theta,z)$, the corresponding plasma density perturbation is $\delta n(r,\theta,z)$. Then the laser vector can be expressed as

$$a=a_s(r,\theta,z)+\delta a(r,\theta,z) \tag{5}$$

assuming the perturbation is in the form of

$$\delta a=\delta_1\exp(i\lambda z)\exp(iN\theta). \tag{6}$$

Here N denotes the azimuthal index of the perturbations, which indicates the number of filaments that the ring can break up. By substituting Eq. (5) into Eq. (1), after some algebra, one can obtain the eigenvalue equation of the perturbation δa:

$$\begin{pmatrix}2ik_L\partial_z+\nabla_\perp^2+\Pi & h-f\frac{a_s^2}{2\gamma_0^2}\\ h^*-f\frac{a_s^{*2}}{2\gamma_0^2} & -2ik_L\partial_z+\nabla_\perp^2+\Pi\end{pmatrix}\begin{pmatrix}\delta a\\ \delta a^*\end{pmatrix}=0. \tag{7}$$

Here $\Pi=k_p^2(F(a_m^2)+F'(a_m^2)a_m^2+f\frac{a_m^2}{2\gamma_0^2})$, $h=F'(a_m^2)a_s^2$, $f=\frac{\frac{N^2}{r_m^2}}{k_p^2+\alpha\frac{N^2}{r_m^2}}$, $F'(u)=\partial_u F$, $\gamma_0=\sqrt{1+a_m^2}$, and a^* and h^* are the conjugates of a and h, respectively. From Eq. (7), one can get the growth rate of the azimuthal modulational instability:

$$\Gamma=\frac{1}{2k_L}\frac{N}{r_m}\sqrt{k_p^2(1+\gamma_0 f)\frac{a_m^2}{\gamma_0^3}-\left(\frac{N}{r_m}\right)^2}. \tag{8}$$

For a cold plasma with $\alpha=0$, the maximum growth rate of the AMI can be expressed as

$$\Gamma_{\max}\simeq\frac{k_p^2}{4k_L}\frac{a_m^2}{\gamma_0^2}. \tag{9}$$

The corresponding maximum number of generated filaments is estimated as follows:

$$N_{\max}\simeq\sqrt{m/2}r_0k_p\frac{a_m}{\sqrt{\gamma_0}}. \tag{10}$$

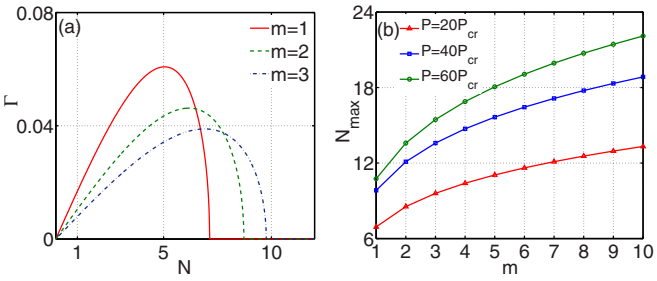

FIG. 1. (a) The growth rate of AMI with different values of topological charge $m = 1,2,3$, where $r_0 = 10\ \mu$m, $n_e = 0.2n_c$, and $P = 20P_{\rm cr}$ are assumed. (b) The maximum number of filaments as a function of m for $P = 20P_{\rm cr}$, $40P_{\rm cr}$, and $60P_{\rm cr}$.

The maximum growth rate of the AMI and maximum number of filaments are plotted in Fig. 1. It is shown from Fig. 1(a) that, for the same input laser power, the maximum growth rate of the AMI is decreased as the topological charge m grows, which indicates that the filamentation process evolves slowly when the topological charge m of optical vortex beams grows. That is, the stable propagation distance before the filamentation occurs can be increased for optical vortex beams with a large value of m. In Fig. 1(b), for the same input power, it can be seen that the number of filaments increases with the topological charge m. For a fixed topological charge m, the number of generated filaments also becomes larger as the input power increases. One can use Eq. (10) to predict the number of filaments in the filamentation process if a set of accurate input laser and plasma parameters of m, r_0, n_e, and a_0 are provided.

III. MULTIPLE FILAMENTS OF RELATIVISTIC OPTICAL VORTEX BEAMS

To understand the filamentation dynamics of optical vortex beams in underdense plasmas, numerical simulations based on the RNSE (1) are conducted [12]. It has been verified that features about the filamentation process of relativistic laser beams in underdense plasmas can be well captured by this physical model [12]. In the simulations, the input laser profile is assumed as follows:

$$a(r,\theta,0) = a_0(1+\delta)\frac{1}{\sqrt{m!}}\left(\frac{\sqrt{2}r}{r_0}\right)^m \exp\left(-\frac{r^2}{r_0^2}\right)\exp(im\theta), \tag{11}$$

where a_0 is the amplitude of the normalized electric field, r_0 is the initial beam waist, $r = \sqrt{x^2+y^2}$, m is the topological charge for the relativistic optical vortex beam, θ is the azimuthal angle, and δ refers to the random perturbation added on the profile, which is generated using the random numbers from the computer. In the simulations, the wavelength is assumed to be 1 μm, the initial beam waist is 10 μm, and the plasma density is $0.2n_c$. The input power of the laser beam ranges from $20P_{\rm cr}$ to $60P_{\rm cr}$. The normalized electron temperature is set as $\alpha = 0$. It has been demonstrated that the thermal effect does not affect the AMI significantly and one can consider the cold plasma for simplicity [12]. Different noise levels [max(δ)] are also considered in the simulations ranging from 0.05 to 0.1.

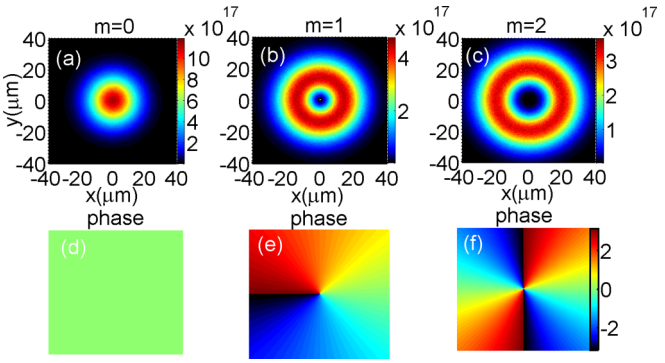

FIG. 2. The initial intensity distribution and the corresponding phase of different optical vortex beams: (a, d) $m = 0$; (b, e) $m = 1$; and (c, f) $m = 2$ with noise level max(δ) = 0.05, where $P = 20P_{cr}$, $r_0 = 10\ \mu$, and $n_e = 0.2n_c$ are taken in the simulations. The unit of the intensity is W/cm^2.

Figure 2 gives the initial intensity and phase distributions of different optical vortex beams with the same input parameters of $P = 20P_{\rm cr}$, $r_0 = 10\ \mu$m, and $n_e = 0.2n_c$. It is shown that the Gaussian laser beam carries no orbital angular momentum; thus, its phase is strictly zero, as shown in Fig. 2(d), whereas for optical vortex beams with $m \neq 0$, it has the characteristics of a singularity and spiral wave front. Its intensity at the center is zero and displays as a ring-shaped structure, as shown in Figs. 2(b) and 2(c). In addition, the optical vortex beam carries a finite orbital angular momentum and its phase ranges from $-\pi$ to π, as shown in Figs. 2(e) and 2(f). During the filamentation process of relativistic optical vortex beams in plasmas, an additional physical quantity, i.e., the orbital angular momentum, should be conserved. This is the main difference between the Gaussian laser beam and the optical vortex beams, which would induce a quite different filamentation process.

The simulation result with the initial conditions given in Fig. 2 is displayed in Fig. 3. The Gaussian laser beam initially experiences a self-focusing stage because of the increase of relativistic electron mass and the ponderomotive expulsions of electrons, as shown in Fig. 3(a). After the self-focusing process, the diffraction ($\nabla_\perp^2$) would gradually exceed the self-focusing effect and play a dominant role. As a result, diffractive rings surrounding a central filament are generated due to the isotropic diffraction, as is exhibited in Fig. 3(d). These rings are unstable modes and would break up into several filaments due to the azimuthal modulation instability, as shown in Fig. 3(g). Finally the laser beam is completely broken up and separated into four filaments. It is noted that the formation and breakup of the ring structures are universal processes during the filamentation stage of Gaussian laser beams [12–14]. Optical vortex beams also undergo an initial self-focusing process. The ring becomes thinner and its amplitude is also increased, as shown in Figs. 3(b) and 3(c). After a relatively long self-focusing distance, the rings begin to break up, as shown in Figs. 3(e) and 3(f). At last, the beam breaks up into several isolated filaments but these filaments are regularly distributed on ring-shaped structures, as shown in Figs. 3(h) and 3(i). By employing Eq. (10) from the perturbation analysis, one can obtain that for the input parameters of $P = 20P_{\rm cr}$,

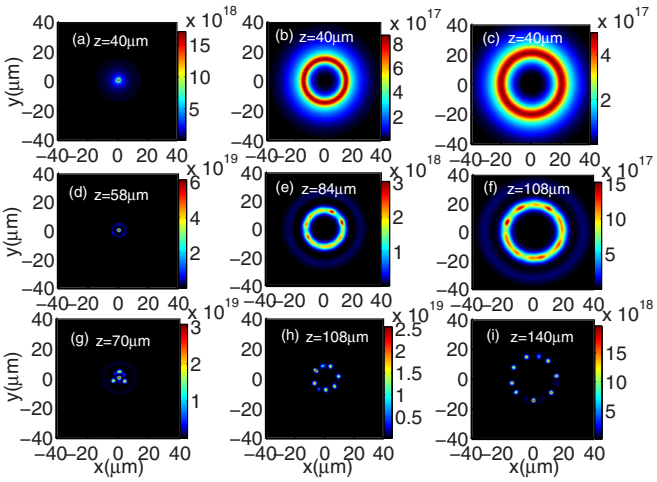

FIG. 3. The intensity patterns at some special positions for the optical vortex beams: (a, d, g) $m = 0$, (b, e, h) $m = 1$, and (c, f, i) $m = 2$. The noise level is set as $\max(\delta) = 0.05$ and the initial parameters with $P = 20P_{cr}$, $r_0 = 10\ \mu$m, and $n_e = 0.2n_c$ are taken. The unit of the intensity is W/cm^2.

$r_0 = 10\ \mu$m, $n_e = 0.2n_c$, and $m = 1$, the maximum number of filaments that can be generated is about seven. This is in good agreement with the simulation result shown in Fig. 3(h). For the optical vortex with $m = 2$, the number of filaments can be estimated as nine, which also agrees well with the simulation result shown in Fig. 3(i). The corresponding evolutions of the maximum intensity with the propagation distance are plotted in Fig. 4. It is shown that both the Gaussian laser beam and the optical vortex beam experience the self-focusing stages. But, compared with the Gaussian laser beam, the self-focusing distance for the optical vortex beam is much increased as the topological charge m grows, as predicted by the theory. On the other hand, the growth rate of the AMI is decreased with the increase of the topological charge. This indicates that the optical vortex beam can experience a relatively long stable propagation distance, and the occurrence

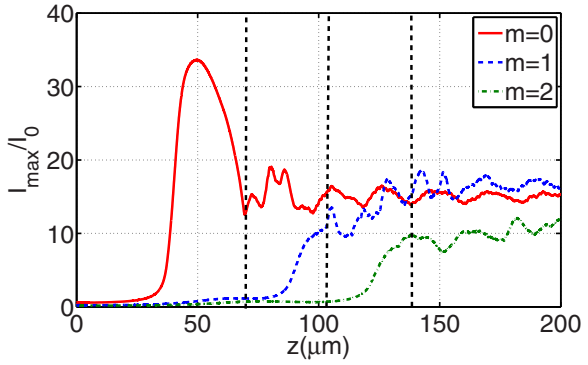

FIG. 4. The evolutions of the maximum intensity with the propagation distance z for $m = 0,1,2$, where the noise level is set as $\max(\delta) = 0.05$, and $P = 20P_{cr}$, $r_0 = 10\ \mu$m, and $n_e = 0.2n_c$ are taken. The dashed lines indicate the distance that the filamentation instability occurs.

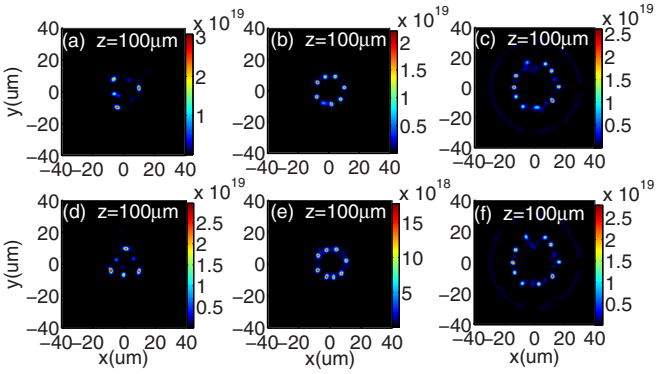

FIG. 5. Filamentation patterns of different optical vortex beams at the same propagation distance with different noise levels of $\max(\delta) = 0.08$ and 0.1 (a, d) for $m = 0$, (b, e) for $m = 1$, and (c, f) for $m = 2$. The initial parameters are the same as in Fig. 3. The unit of the intensity is W/cm^2.

of the subsequent filamentation process can be delayed by increasing the topological charge, as shown in Fig. 4.

Since the filamentation process is a noise-induced process, the number and location of the multiple filaments of Gaussian laser beams are unpredictable from shot to shot at different noise levels. The simulation result with different noise levels is displayed in Fig. 5. For the Gaussian laser beam, one can clearly see that the filaments are randomly distributed at different noise levels, as shown in Figs. 5(a) and 5(d), whereas for optical vortex beams with a finite orbital angular momentum, the total angular momentum is conserved during its propagation. As a result, the generated filaments are regularly distributed on the rings and the whole beam rotates along the laser axis during the propagation. In this case, the location and number of the filaments are not sensitive to the initial beam perturbation. The placement of individual filaments is approximately deterministic and the number of filaments is almost fixed, as shown in Figs. 5(b), 5(c), 5(e), and 5(f). It is shown that, even when the noise level reaches 0.1, the filaments in Figs. 5(e) and 5(f) are still tightly located on the ring and the number of filaments approximately remains the same value as that in Figs. 5(b) and 5(c).

To demonstrate the characteristics of the filamentation process of relativistic optical vortex beams in plasmas, different input powers and topological charges are also chosen in the simulations. The simulation result is shown in Fig. 6. It can be seen that, with increasing the input power, the number of filaments is increased and the filamentation process also occurs at a shorter propagation distance. This is due to the reduction of the self-focusing distance, which is inversely proportional to the input laser power. In addition, it is noted that for the given topological charge $m = 1$ with different input powers of $P = 20P_{cr}$, $40P_{cr}$, and $60P_{cr}$ the corresponding numbers of generated filaments are about 7, 9, and 11, respectively, as shown in Figs. 6(a), 6(d), and 6(g). This is in good agreement with the theoretical predictions given in Fig. 1(b). For a fixed input power, for example, $P = 40P_{cr}$, a larger topological charge always corresponds to a larger number of filaments; as shown in Figs. 6(d)–6(f), the number of filaments is about 10, 12, and 14 for $m = 1$, 2, and 3, respectively. This also

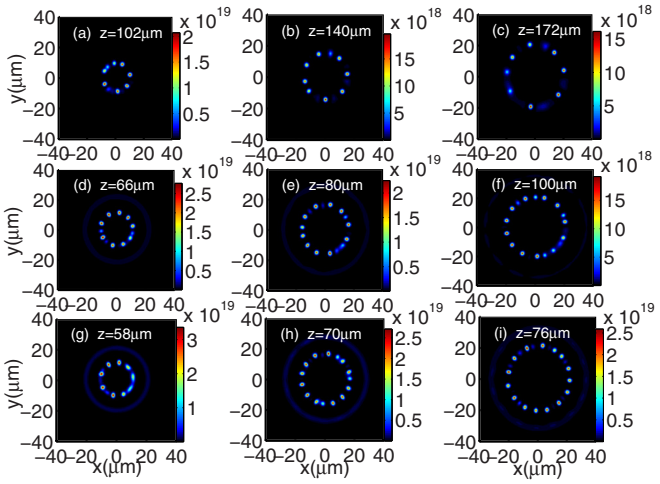

FIG. 6. Filamentation patterns of different optical vortex beams with different input powers and topological charge m (a–c) for $P = 20P_{cr}$, $m = 1$, 2, and 3; (d–f) for $P = 40P_{cr}$, $m = 1$, 2, and 3; and (g–i) for $P = 60P_{cr}$, $m = 1$, 2, and 3. The initial parameters are set as $\max(\delta) = 0.05$, $r_0 = 10\,\mu$m, and $n_e = 0.2n_c$. The unit of the intensity is W/cm^2.

agrees well with the blue line shown in Fig. 1(b). Thus for the filamentation process of relativistic optical vortex beams in underdense plasmas, one can employ Eq. (10) to well predict the number of filaments that can be generated. That is, the filamentation process is controllable by employing relativistic optical vortex beams in plasmas.

IV. SUMMARY

It is a crucial problem to manipulate the filamentation instability of relativistic laser pulses in plasmas as it underpins many applications in laser plasma physics. In our earlier work, we demonstrated that the filamentation process can be mitigated by employing an elliptically distributed laser beam, which experiences an anisotropic diffraction process, and the formation of the uncontrollable diffractive rings is suppressed. As a result, the laser beam breaks up into a regular filamentation pattern with most of its energy concentrated in a central filament. Here we propose an alternative method to manipulate the laser filamentation process in plasmas by using optical vortex beams. It is shown that the optical vortex beam can go through a longer stable self-focusing stage in comparison to the Gaussian laser beam as its topological charge grows. In addition, during the filamentation stage, the optical vortex beam exhibits a very robust behavior. Its filamentation patterns are regularly distributed on a ring and the number of filaments is predictable. Under the constraint of laser orbital angular momentum conservation, the number and location of filaments are unsensitive to initial beam noise. In contrast to the random filamentation process of the Gaussian laser beam, the filamentation process for the optical vortex beam can be controllable. Such a well-organized laser beam should be of great interest for many potential applications in relativistic high-energy-density plasmas. Since generation of relativistic optical vortex beams can be implemented by techniques such as multilevel spiral phase plate, stimulated Raman amplification, light fans, etc., it should therefore be possible to set up new experiments in the future to examine our simulation results. Furthermore, it is noted that such an optical vortex beam with finite orbital angular momentum also creates great interest in broad contexts including vortex electron beams and vortex x-ray generation [22,49].

ACKNOWLEDGMENTS

This work is supported by the National Key Research and Development Program No. 2016YFA00401101, the National Natural Science Foundation of China (Grants No. 91230205, No. 11575031, and No. 11575298), the National Basic Research 973 Project, No. 2013CB834100, and the National High-Tech 863 Project. The authors would like to thank C. Z. Xiao, K. Q. Pan, Z. Xu, H. X. Chang, W. P. Yao, Y. X. Zhang, X. R. Xu, Q. S. Feng, H. C. Zhang, and J. X. Gong for their useful discussions and help.

[1] M. Tabak, J. Hammer, M. E. Glinsky, W. L. Kruer, S. C. Wilks, J. Woodworth, E. M. Campbell, M. D. Perry, and R. J. Mason, Phys. Plasmas **1**, 1626 (1994).

[2] A. J. Kemp, F. Fiuza, A. Debayle, T. Johzaki, W. B. Mori, P. K. Patel, Y. Sentoku, and L. O. Silva, Nucl. Fusion **54**, 054002 (2014).

[3] E. Esarey, C. B. Schroeder, and W. P. Leemans, Rev. Mod. Phys. **81**, 1229 (2009).

[4] A. P. L. Robinson, A. V. Arefiev, and D. Neely, Phys. Rev. Lett. **111**, 065002 (2013).

[5] C. T. Zhou and X. T. He, Appl. Phys. Lett. **90**, 031503 (2007); C. T. Zhou, L. Y. Chew, and X. T. He, He, *ibid.* **97**, 051502 (2010).

[6] J. Fuchs, Y. Sentoku, S. Karsch, J. Cobble, P. Audebert, A. Kemp, A. Nikroo, P. Antici, E. Brambrink, A. Blazevic, E. M. Campbell, J. C. Fernández, J.-C. Gauthier, M. Geissel, M. Hegelich, H. Pépin, H. Popescu, N. Renard-LeGalloudec, M. Roth, J. Schreiber, R. Stephens, and T. E. Cowan, Phys. Rev. Lett. **94**, 045004 (2005).

[7] R. M. G. M. Trines, F. Fiuza, R. Bingham, R. A. Fonseca, L. O. Silva, R. A. Cairns, and P. A. Norreys, Nat. Physics **7**, 87 (2011).

[8] G. Z. Sun, E. Ott, Y. C. Lee, and P. Guzdar, Phys. Fluids **30**, 526 (1987); X. L. Chen and R. N. Sudan, Phys. Rev. Lett. **70**, 2082 (1993).

[9] C. T. Zhou and X. T. He, Phys. Rev. E **49**, 4417 (1994); C. T. Zhou, X. T. He, and T. X. Cai, *ibid.* **50**, 4136 (1994); C. T. Zhou, M. Y. Yu, and X. T. He, *ibid.* **73**, 026209 (2006).

[10] M. D. Feit, A. M. Komashko, S. L. Musher, A. M. Rubenchik, and S. K. Turitsyn, Phys. Rev. E **57**, 7122 (1998); A. Kim, M. Tushentsov, F. Cattani, D. Anderson, and M. Lisak, *ibid.* **65**, 036416 (2002).

[11] B. Qiao, C. H. Lai, and C. T. Zhou, Appl. Phys. Lett. **91**, 221114 (2007); Phys. Plasmas **14**, 112301 (2007).

[12] T. W. Huang, C. T. Zhou, A. P. L. Robinson, B. Qiao, H. Zhang, S. Z. Wu, H. B. Zhuo, P. A. Norreys, and X. T. He, Phys. Rev. E **92**, 053106 (2015).

[13] A. B. Borisov, A. V. Borovskiy, O. B. Shiryaev, V. V. Korobkin, A. M. Prokhorov, J. C. Solem, T. S. Luk, K. Boyer, and C. K. Rhodes, Phys. Rev. A **45**, 5830 (1992); A. B. Borisov, A. V. Borovskiy, A. Mcpherson, K. Boyer, and C. K. Rhodes, Plasma Phys. Control. Fusion **37**, 569 (1995).
[14] A. Pukhov and J. Meyer-ter-Vehn, Phys. Rev. Lett. **76**, 3975 (1996).
[15] K. A. Tanaka, M. M. Allen, A. Pukhov, R. Kodama, H. Fujita, Y. Kato, T. Kawasaki, Y. Kitagawa, K. Mima, N. Morio, H. Shiraga, M. Iwata, T. Miyakoshi, and T. Yamanaka, Phys. Rev. E **62**, 2672 (2000).
[16] N. E. Andreev, L. M. Gorbunov, P. Mora, and R. R. Ramazashvili, Phys. Plasmas **14**, 083104 (2007).
[17] M. Borghesi, A. J. MacKinnon, L. Barringer, R. Gaillard, L. A. Gizzi, C. Meyer, O. Willi, A. Pukhov, and J. Meyer-ter-Vehn, Phys. Rev. Lett. **78**, 879 (1997).
[18] G. Li, R. Yan, C. Ren, T.-L. Wang, J. Tonge, and W. B. Mori, Phys. Rev. Lett. **100**, 125002 (2008).
[19] G. Li, W. B. Mori, and C. Ren, Phys. Rev. Lett. **110**, 155002 (2013).
[20] A. G. MacPhee, L. Divol, A. J. Kemp, K. U. Akli, F. N. Beg, C. D. Chen, H. Chen, D. S. Hey, R. J. Fedosejevs, R. R. Freeman, M. Henesian, M. H. Key, S. Le Pape, A. Link, T. Ma, A. J. Mackinnon, V. M. Ovchinnikov, P. K. Patel, T. W. Phillips, R. B. Stephens, M. Tabak, R. Town, Y. Y. Tsui, L. D. Van Woerkom, M. S. Wei, and S. C. Wilks, Phys. Rev. Lett. **104**, 055002 (2010).
[21] L. Allen, M. W. Beijersbergen, R. J. C. Spreeuw, and J. P. Woerdman, Phys. Rev. A **45**, 8185 (1992).
[22] B. J. McMorran, A. Agrawal, I. M. Anderson, A. A. Herzing, H. J. Lezec, J. J. McClelland, and John Unguris, Science **331**, 192 (2011).
[23] L. K. Zhang and P. L. Marston, Phys. Rev. E **84**, 065601 (2011).
[24] J. L. Thomas and R. Marchiano, Phys. Rev. Lett. **91**, 244302 (2003).
[25] M. Padgett and R. Bowman, Nat. Photonics **5**, 343 (2011).
[26] J. Wang, J. Y. Yang, I. M. Fazal, N. Ahmed, Y. Yan, H. Huang, Y.X. Ren, Y. Yue, S. Dolinar, M. Tur, and A. E. Willner, Nat. Photonics **6**, 488 (2012).
[27] G. Molina-Terriza, J. P. Torres, and L. Torner, Nat. Phys. **3**, 305 (2007).
[28] F. Tamburini, B. Thidé, and G. Molina, Nat. Phys. **7**, 195 (2011).
[29] Marin Soljačić, Suzanne Sears, and Mordechai Segev, Phys. Rev. Lett. **81**, 22 (1998).
[30] G. Mechain, A. Couairon, M. Franco, B. Prade, and A. Mysyrowicz, Phys. Rev. Lett. **93**, 035003 (2004).
[31] A. Dubietis, G. Tamosauskas, G. Fibich, and B. Ilan, Opt. Lett. **29**, 1126 (2004); G. Fibich, S. Eisenmann, B. Ilan, and A. Zigler, *ibid.* **29**, 1772 (2004).
[32] W. J. Firth and D. V. Skryabin, Phys. Rev. Lett. **79**, 2450 (1997).
[33] D. Mihalache, D. Mazilu, L.-C. Crasovan, B. A. Malomed, and F. Lederer, Phys. Rev. E **61**, 7142 (2000).
[34] L. T. Vuong, T. D. Grow, A. Ishaaya, A. L. Gaeta, G. W. 't Hooft, E. R. Eliel, and G. Fibich, Phys. Rev. Lett. **96**, 133901 (2006).
[35] A. Vinçotte and L. Bergé, Phys. Rev. Lett. **95**, 193901 (2005).
[36] N. K. Efremidis, K. Hizanidis, B. A. Malomed, and P. Di Trapani, Phys. Rev. Lett. **98**, 113901 (2007).
[37] P. Polynkin, C. Ament, and J. V. Moloney, Phys. Rev. Lett. **111**, 023901 (2013).
[38] M. W. Beijersbergen, L. Allen, H. E. L. O. van der Veen, and J. P. Woerdman, Opt. Commun. **96**, 123 (1993).
[39] G. A. Turnbull, D. A. Robertson, G. M. Smith, L. Allen, and M. J. Padgett, Opt. Commun. **127**, 183 (1996).
[40] N. R. Heckenberg, R. McDuff, C. P. Smith, H. Rubinsztein-Dunlop, and M. J. Wegener, Opt. Quantum Electron. **24**, S951 (1992).
[41] K. Sueda, G. Miyaji, N. Miyanaga, and M. Nakatsuka, Opt. Express **12**, 3548 (2004).
[42] J. Vieira, R. M. G. M. Trines, E. P. Alves, R. A. Fonseca, J. T. Mendonça, R. Bingham, P. Norreys, and L. O. Silva, Nat. Commun. **7**, 10371 (2016).
[43] Y. Shi, B. F. Shen, L. G. Zhang, X. M. Zhang, W. P. Wang, and Z. Z. Xu, Phys. Rev. Lett. **112**, 235001 (2014).
[44] J. T. Mendonça and J. Vieira, Phys. Plasmas **21**, 033107 (2014); J. Vieira and J. T. Mendonça, Phys. Rev. Lett. **112**, 215001 (2014).
[45] X. M. Zhang, B. F. Shen, L. G. Zhang, J. C. Xu, X. F. Wang, W. P. Wang, L. Q. Yi, and Y. Shi, New J. Phys. **16**, 123051 (2014); X. M. Zhang, B. F. Shen, Y. Shi, X. F. Wang, L. G. Zhang, W. P. Wang, J. C. Xu, L. Q. Yi, and Z. Z. Xu, Phys. Rev. Lett. **114**, 173901 (2015).
[46] C. Brabetz, S. Busold, T. Cowan, O. Deppert, D. Jahn, O. Kester, M. Roth, D. Schumacher, and V. Bagnoud, Phys. Plasma **22**, 013105 (2015).
[47] T. Mizumachi, Adv. Differ. Equ. **12**, 241 (2007).
[48] G. Fibich and N. Gavish, Phys. Rev. A **77**, 045803 (2008).
[49] E. Hemsing, A. Knyazik, M. Dunning, D. Xiang, A. Marinelli, C. Hast, and J. B. Rosenzweig, Nat. Phys. **9**, 549 (2013); E. Hemsing, M. Dunning, C. Hast, T. Raubenheimer, and D. Xiang, Phys. Rev. Lett. **113**, 134803 (2014).